Nuclear Compton scattering from ^{12}C and bound-nucleon polarizabilities

B. J. Warkentin, D. L. Hornidge, R. Igarashi, J. C. Bergstrom, E. L. Hallin, N. R. Kolb, R. E. Pywell, D. M. Skopik, and J. M. Vogt
Department of Physics and Engineering Physics, University of Saskatchewan, Saskatoon, Saskatchewan, Canada S7N 5E2

G. Feldman
Department of Physics, The George Washington University, Washington, D.C. 20052
(Received 19 January 2001; published 4 June 2001)

Compton scattering cross sections from ^{12}C have been measured at scattering angles of $\theta_\gamma = 35° - 150°$ using tagged photons of $E_\gamma = 84 - 105$ MeV. Attempts to extract nucleon polarizabilities from the data were hampered by model ambiguities. These included uncertainties in the strength of the electric quadrupole and quasideuteron total photon absorption channels, and in the parametrizations of meson-exchange effects and nuclear form factors. These ambiguities led to large variations in the extracted values of the effective polarizabilities of the bound nucleon. Inelastic Compton scattering cross sections from the 4.44 MeV first-excited state were also obtained.

DOI: 10.1103/PhysRevC.64.014603 PACS number(s): 25.20.Dc, 13.40.Em, 13.60.Fz, 14.20.Dh

I. INTRODUCTION

Considerable attention in intermediate-energy nuclear physics has been recently focused on the electric and magnetic polarizabilities of the nucleon, $\bar{\alpha}$ and $\bar{\beta}$. The polarizabilities represent first-order responses of internal structure to external electric and magnetic fields. Two questions of interest arise: what are the polarizabilities of the free nucleon, and are these values altered when the nucleon is within a nucleus?

In the case of the proton, the elastic photon scattering, or nuclear Compton scattering (NCS), cross sections below incident energies of about 100 MeV can be well described by the low-energy expansion (LEX). In the LEX the deviation from the Born cross section for point particles is manifest in terms proportional to E_γ^2 involving the polarizabilities. Scattering at forward angles is sensitive to the sum $(\bar{\alpha}+\bar{\beta})_p$, while at backward angles the difference $(\bar{\alpha}-\bar{\beta})_p$ dominates. Through application of dispersion relations the sum is constrained, leaving the difference as the only free parameter. Global averages of the sum and difference obtained from numerous proton Compton scattering experiments have been given in Ref. [1],

$$(\bar{\alpha}-\bar{\beta})_p = 10.0 \pm 1.5 \pm 0.9, \tag{1}$$

$$(\bar{\alpha}+\bar{\beta})_p = 15.2 \pm 2.6 \pm 0.2, \tag{2}$$

and more recently in Ref. [2],

$$(\bar{\alpha}-\bar{\beta})_p = 10.1 \pm 1.7^{+1.2}_{-0.9}, \tag{3}$$

$$(\bar{\alpha}+\bar{\beta})_p = 13.2 \pm 0.9^{+0.2}_{-0.5}. \tag{4}$$

In Eqs. (1)–(4), the first error is the combined statistical and systematic, and the second is due to the model dependence of the dispersion-relation extraction method. The units for the polarizabilities are 10^{-4} fm^3. When combined with the standard Baldin dispersion-relation sum rule [3],

$$(\bar{\alpha}+\bar{\beta})_p = 14.2 \pm 0.5, \tag{5}$$

Eq. (3) leads to values of

$$\bar{\alpha}_p = 12.1 \pm 0.9 \pm 0.6, \quad \bar{\beta}_p = 2.1 \mp 0.9 \mp 0.6. \tag{6}$$

Recent reevaluations of the sum rule yield 13.69 ± 0.14 [4] and 14.0 ± 0.5 [5]. All evaluations are in agreement with the measured values within errors.

A similar sum rule is available for the neutron [6],

$$(\bar{\alpha}+\bar{\beta})_n = 15.8 \pm 0.5 \tag{7}$$

(with recent reevaluations of 14.40 ± 0.66 [4] and 15.2 ± 0.5 [5]). However, direct Compton scattering measurements are not possible, so the extraction of neutron polarizabilities is more complicated and current values are highly uncertain. Previous determinations of the static polarizability α_n from experiments involving low-energy neutron scattering from a heavy nucleus are inconsistent [7–9]. Similarly, earlier measurements of quasifree and Compton scattering from the deuteron [10,11] have been plagued by large uncertainties. Recent measurements of quasifree Compton scattering from the deuteron for the proton, $d(\gamma,\gamma p)n$, at Mainz gave

$$(\bar{\alpha}-\bar{\beta})_p = 9.1 \pm 1.7 \pm 1.2 \quad [12], \tag{8}$$

which is consistent with the free proton. This suggests little medium modification. For the neutron, $d(\gamma,\gamma n)p$ at Saskatchewan Accelerator Laboratory (SAL) gave

$$(\bar{\alpha}-\bar{\beta})_n = 0 - 12.8 \quad [13]. \tag{9}$$

The upper limit in Eq. (9) was obtained by using the results of Ref. [10] as a constraint. This is consistent with the free-proton difference. Based on the value for the difference in

Eq. (9) and the sum-rule constraint in Eq. (7), the neutron polarizabilities are within the ranges

$$\bar{\alpha}_n = 7.9 - 14.3, \quad \bar{\beta}_n = 7.9 - 1.5. \tag{10}$$

Equations (6) and (10) can be used to calculate the proton-neutron-averaged polarizabilities,

$$\bar{\alpha}_N = 9.2 - 14.0, \quad \bar{\beta}_N = 5.8 - 1.0, \tag{11}$$

and the corresponding isospin-averaged difference,

$$(\bar{\alpha} - \bar{\beta})_N = 3.4 - 13.0. \tag{12}$$

From the sum rules, Eqs. (5) and (7), the isospin-averaged sum is

$$(\bar{\alpha} + \bar{\beta})_N = 15.0 \pm 0.5. \tag{13}$$

These values can then be compared to a recent measurement of Compton scattering from the deuteron [14], the simplest composite nucleus. This experiment yielded

$$(\bar{\alpha} - \bar{\beta})_N = 2.2 \pm 1.8, \tag{14}$$

which is just consistent with the isospin average [Eq. (12)]. However, it is not consistent with predictions that the neutron and proton polarizabilities should be similar (e.g., chiral perturbation theory [15]). This suggests that there was missing physics in the calculations used to extract the polarizabilities.

The Compton scattering from more complex nuclei can be parametrized in a relatively model-independent way below the pion threshold in terms of polarizability constants, provided the total photoabsorption cross section and its multipole composition are known. These effective polarizabilities, $\tilde{\alpha}_{eff}$ and $\tilde{\beta}_{eff}$, may include deviations from the free-nucleon values $(\Delta\bar{\alpha}, \Delta\bar{\beta})$ due to the possible effects of nuclear binding and meson-exchange currents, such that

$$\tilde{\alpha}_{eff} = \bar{\alpha}_N + \Delta\bar{\alpha}, \quad \tilde{\beta}_{eff} = \bar{\beta}_N + \Delta\bar{\beta}. \tag{15}$$

Furthermore, some theoretical [16] and preliminary experimental [17] studies suggested the possibility that medium modifications, such as alteration of the virtual pion cloud surrounding the nucleon quark core and Pauli blocking or swelling of the nucleon radius, result in a sum for $\tilde{\alpha}_{eff} + \tilde{\beta}_{eff}$, which is somewhat different from the free-nucleon-averaged sum. However, recent nuclear Compton scattering measurements of this sum [18–20] have been consistent with the free-nucleon value.

On the other hand, these same measurements disagree about whether $\tilde{\alpha}_{eff}$ and $\tilde{\beta}_{eff}$ are individually the same as their free-nucleon counterparts. Experiments done at Illinois and SAL on ^{16}O at energies from 27 to 108 MeV [20], and at MAX-LAB (Lund) on ^{4}He at 87 MeV [21], both implied a large decrease in the relative strength of the effective electric polarizability, $\Delta\bar{\alpha} \approx -8.5$ [using $\bar{\alpha}_N$ from Eq. (11)]. In contrast, a study by the same Lund/Göttingen group on ^{12}C and ^{16}O at energies of 58 and 75 MeV [18] determined that the effective bound and free values were essentially the same. Their most recent experiment using ^{40}Ca at energies of 58 and 74 MeV and ^{16}O and ^{4}He at 61 MeV [22] again suggested that the modifications are much smaller than that observed in Ref. [20], and were consistent with the meson-exchange corrections calculated by Hütt and Milstein [23] of $\Delta\bar{\alpha} \approx -2, -1, 0$ for ^{40}Ca, ^{16}O, and ^{4}He, respectively. Proff *et al.* [22] further proposed that their earlier data on ^{4}He [21], which employed untagged bremsstrahlung, could justifiably be discarded because of the inherent uncertainties in the analysis of this type of experiment. However, there still remains a disagreement in the cross sections measured at backward angles between this newer ^{4}He [22] measurement and an earlier tagged measurement on ^{4}He performed by Wells [24].

II. EXPERIMENT

The present experiment (complete details can be found in [25]) was conducted at the Saskatchewan Accelerator Laboratory. An electron beam energy of 135 MeV was chosen to avoid neutral particle background arising from pion photoproduction. The duty factor over the course of the experiment was greater than 40%. Incident photon energies of 84–105 MeV were tagged in the 62-channel SAL tagger [26] by the standard technique. Tagging efficiencies were measured approximately once every 8 h by placing a lead-glass detector directly in a flux-reduced photon beam. This measured the fraction of tagged photons passing through the defining collimators, which averaged $(53.5 \pm 0.5)\%$.

Photons scattered from a 8.22 ± 0.04-g/cm^2 block of graphite were detected in BUNI (Boston University NaI) [27], a NaI detector capable of high detection efficiency and excellent energy resolution due to its size and uniformity characteristics. BUNI's 2% energy resolution allowed the discrimination of elastic and inelastic (from the 4.44 MeV first-excited state) contributions to the yield. BUNI consists of 11 optically isolated scintillator elements: a cylindrical NaI core measuring 26.7 cm in diameter and 55.9 cm in length, four NaI quadrants that form a 10.8-cm-thick annulus of the same length, and six plastic scintillator segments that constitute an outer annulus with a length of 51.0 cm and a thickness of 12.7 cm. This was surrounded by 28 cm of lead and steel shielding to suppress the electromagnetic and neutron background that can overwhelm the low data rates of nuclear Compton scattering or degrade detector resolution by pileup.

The sum of the energy deposited in the core and the quadrants was used to define the energy of a scattered photon event. A zero-degree-calibration run and quadrant-calibration runs were used in conjunction with a gain-tracking system to determine the gains of BUNI's photomultiplier tubes [28]. The zero-degree measurement, placing BUNI directly in the current-reduced beam, was performed once during the experiment. Quadrant calibrations were performed daily with a Thorium-C source. The gain-tracking system consisted of a 2-in. NaI detector, a light-emitting diode that periodically sent light pulses to both BUNI and the small NaI via fiber-

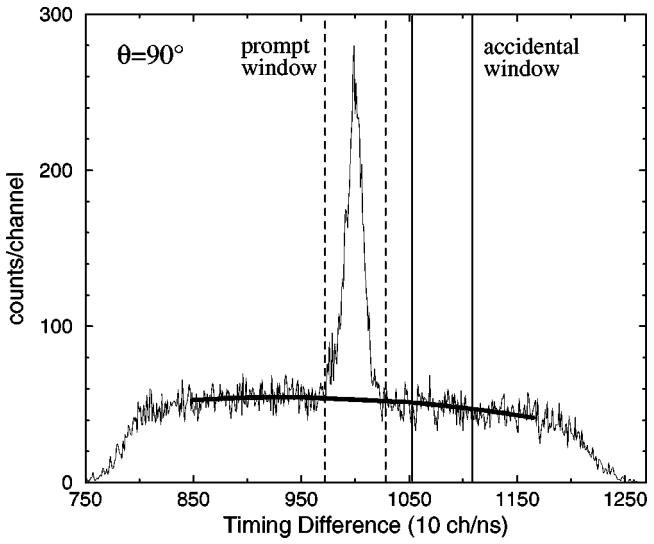

FIG. 1. TDC spectrum of coincidences between the tagger focal plane and BUNI. The solid line is the quadratic fit to the accidental spectrum.

optic cables, and a Thorium-C source positioned proximally to the small NaI.

Data were acquired with BUNI placed at laboratory scattering angles of 35°, 60°, 90°, 120°, and 150°. The solid angles subtended by the (12.7 ± 0.1)-cm-diameter collimator in front of BUNI were estimated to be 8.37, 8.51, 15.97, 8.51, and 7.98 msr using EGS4 (Electron Gamma Shower) software simulations. The uncertainty in the aperture diameter accounted for most of the estimated uncertainty of 1.8% in the solid angles.

III. ANALYSIS

Before cross sections could be extracted, energy spectra were subject to background rejection and subtraction. The outer plastic annulus of BUNI, and six additional 2.54-cm-thick plastic scintillator paddles covering the front and back of BUNI, were used to veto charged-particle background, particularly cosmic rays. Cosmic rays also deposit a disproportionate amount of energy in BUNI's quadrants relative to the core compared to scattered photon events. Hence, it was possible to eliminate 99.7% of cosmic rays based on the plastic-scintillator veto and the ratio of energy depositions. The cut on the veto counter at the front of BUNI was also important in rejecting charged particles entering through the aperture of BUNI.

Events surviving the above set of cuts were then subject to a cut on the time-to-digital converter (TDC) spectrum (see Fig. 1) measuring the timing of coincidences between the tagger focal-plane and BUNI. Energy spectra corresponding to two timing windows were accumulated: a ''prompt'' spectrum for events whose timing fell within a 5.6-ns window that included the peak corresponding to tagged scattered photon events, and an ''accidental'' spectrum for those events within a window of equal width to the right of the prompt window, where only random coincidences (with untagged reactions) are expected to occur. Then the underlying accidental background was subtracted from the prompt spectrum for a net spectrum,

$$\text{net} = \text{prompts} - \eta \times \text{accidentals}, \tag{16}$$

where η is a correction factor calculated from a quadratic fit used to account for the fact that the accidental part of the TDC spectrum is not flat at the tagger rates and duty factors used in this experiment. In addition to accidental reaction products, neutrons produced from tagged photons appear to the left of the prompt window and were excluded from the spectra by these TDC windows.

For the final scattered photon spectra (see Fig. 2), contributions from tagged scattered photons originating from other than the ^{12}C target had to be removed. For this purpose, yields were measured with the target removed from the beam line. These ''target-out'' yields were consistent with zero. However, these yields were still subtracted (scaled appropriately by the respective incident fluxes) from the ''target-in'' yields in order to properly calculate the statistical uncertainties.

To calculate the elastic cross sections, the net energy spectra were integrated within a 6-MeV region of interest (ROI), delimited by the vertical lines in Fig 2. The left limit of the ROI was restricted by the existence of the inelastic peak. Normalizing this raw yield of elastic-scattered photons required calculating the detection efficiency of this ROI, ε_{ROI}, i.e., the fraction of counts in the same ROI from the total in the response line shape. Using the detector response line shape, two peaks were simultaneously fit to the spectra, one for the elastic peak and another for the inelastic peak located 4.4 MeV lower in energy. Thus, the fit parameters included two scaling factors (of the response line shape) measuring the strength of the elastic and inelastic contributions, and an energy-shift parameter used to align the response line shape with the elastic peak of the scattered spectrum. At the forward scattering angles of 35° and 60°, the fits also included a smooth atomic background function.

In performing the fits, two line shape variants were considered: the detector response measured from the data of the zero-degree run, and an EGS-simulated spectrum with the detector positioned at the appropriate scattering angle (see Fig. 3). Fits to the final spectra with these two types of line shapes resulted in very similar reduced χ^2 (e.g., at 90°, the χ^2_ν was 1.26 and 1.20, respectively), and no variant with predominantly lower χ^2, over the range of angles. This indicated that there was no clear preference between the two line shapes. The final ε_{ROI} was the median value giving values of about 83%. In addition to the deviation in this average, the estimated errors in ε_{ROI} of 1.5–3.1 % include consideration of shifts in the gain calibration and changes to the line shape (e.g., broadening of the line shape by convolution with a Gaussian). Based on the fits, atomic background accounted for 2.6% and 0.7% of the number of counts integrated within the ROI in the scattered photon spectra at 35° and 60°, respectively.

At the high photon-flux rates used, detection of more than one photon in BUNI per event, or pileup, was a potential

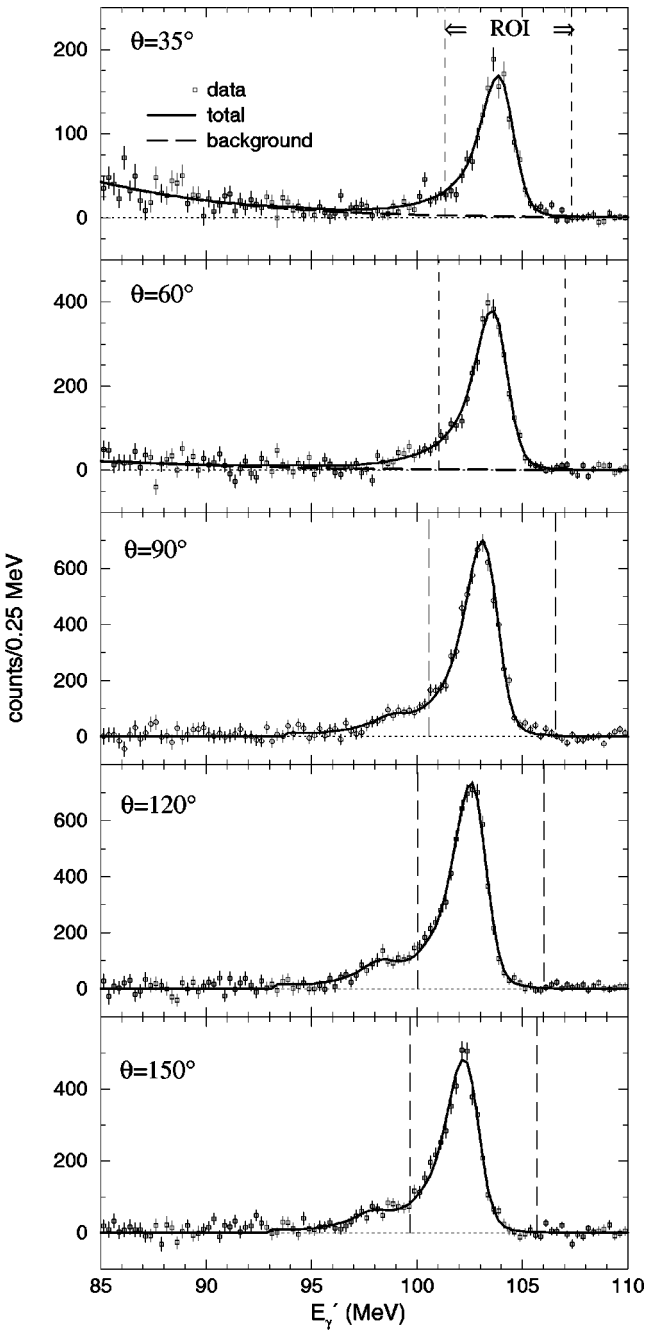

FIG. 2. Energy spectra for scattered photons for the full focal plane (84–105 MeV). The ''total'' line refers to a fit to the elastic and inelastic peaks and the atomic background (at $\theta = 35°, 60°$). The fit shown used the zero-degree data as the detector-response line shape.

concern as an effect on energy resolution and ROI determinations. Pileup was monitored by using a random trigger to sample the energy deposition in BUNI due purely to background and this was used to determine corrections. The choice of the 6-MeV ROI for the integration, extending beyond the high-energy side of the response function, was advantageous because it was wide enough to minimize the effect of pileup. Thus, pileup effects were rendered negligible: the corrections were less than 0.4% for all scattering angles.

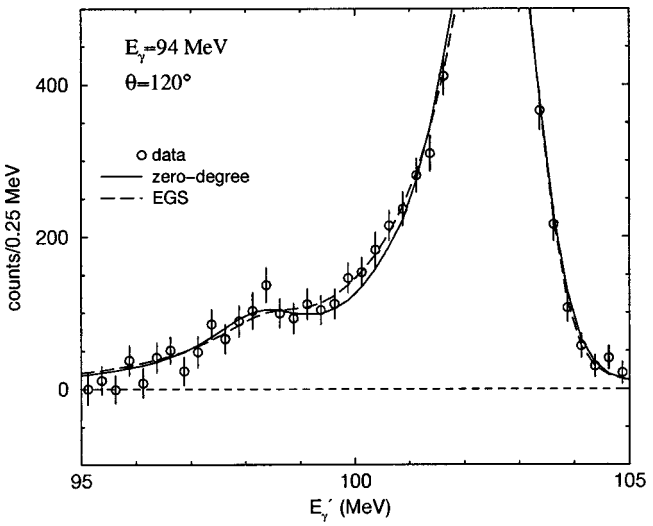

FIG. 3. Comparison between use of the zero-degree data and the EGS-simulated scattered-photon spectra as the response line shape in the fits to the energy spectrum.

The inelastic cross sections were obtained from the ratio of the inelastic to elastic peaks in the fits to the energy spectra (see Fig. 2). The errors in the inelastic cross sections included the uncertainties in the fitting parameters. While the difference in the zero-degree data and EGS-simulated line shapes had only a small effect on the elastic cross sections, it had a very large impact on the inelastic values. For example, at 120° the fit using the zero-degree line shape suggested that the 4.4-MeV inelastic value was 7.4% of the elastic value, while use of the EGS-simulated line shape yielded 4.7%. As with ε_{ROI}, the median value of the inelastic cross section using each line shape was calculated. The dominant systematic error was the deviation in this average. The presence of the electromagnetic background rendered the extraction of the inelastic cross section at 35° unreliable.

Normalization of the cross sections also entailed determination of the overall photon-absorption efficiency factor, ε_{abs}, which ranged from 80.2–82.2 %. This included the attenuation of both the incident and scattered photons in the ^{12}C target, as well as the loss of photons due to their conversion to electrons in the air and particularly the plastic scintillators before reaching the NaI of BUNI. The factor was calculated using the zero-degree data, its corresponding tagging efficiency run, and EGS simulations.

The relatively high tagger rates also meant that rate-dependent effects needed to be considered. Corrections for ''stolen coincidences'' (a prompt hit on a tagger channel preempted by an earlier accidental hit on the same channel) and false additional hits in adjacent tagger channels, were calculated. For the measurements at 35°, 60°, 90°, 120°, and 150°, the instantaneous rates (i.e., avg rate/duty factor) averaged over the 62-channel focal plane were 0.35, 0.85, 1.26, 1.37, and 1.08 MHz, respectively. The rates at forward scattering angles were reduced, because of the increased electromagnetic background, to maintain sufficiently low levels of pileup and deadtime. Calculation of the tagger rate-

TABLE I. Differential cross sections (lab frame) for the elastic scattering of 84–105 MeV photons from ^{12}C. Values are listed for the sum over the entire focal plane (E_γ=94 MeV) and for the four subdivisions (E_γ=86, 92, 97, and 102 MeV). The first error is statistical and the second is systematic.

θ (deg)	$d\sigma/d\Omega$ (nb/sr)				
	94 MeV	86 MeV	92 MeV	97 MeV	102 MeV
35	567±17±19	656±38±27	633±34±26	493±33±19	454±31±18
60	363±8±11	425±18±16	380±16±13	337±15±11	292±15±10
90	292±5±10	347±11±14	300±10±11	256±9±9	252±9±9
120	340±6±10	419±12±15	349±11±12	290±11±10	282±11±9
150	323±7±10	407±15±15	327±12±11	277±13±10	256±12±10

dependent effects indicated that the measured cross sections at 35°–150° should be increased by 0.9%, 1.9%, 3.0%, 3.1%, and 2.3%.

The elastic cross sections are given in Table I. In addition to the cross section at 94 MeV, which represents the sum over the entire tagger focal plane, it was also feasible to subdivide the focal plane into four energy bins centered at 102, 97, 92, and 86 MeV. The statistical uncertainties correspond to one standard deviation in counting statistics. Total systematic errors were 3.0–4.2 %. These consisted of the estimated uncertainties in the target thickness (0.5%), solid angle (1.8%), incident flux (1.0%), absorption effects factor ε_{abs} (1.3%), rate-dependent effects (0.4–1.6 %, depending on angle), atomic background and pileup corrections (0.4–1.1 %), and normalization factor ε_{ROI} (1.5–3.1 %).

The inelastic cross sections for the 4.4-MeV excitation are tabulated in Table II. The large systematic error (20–100 %) is dominated by the differences between the fits to the energy spectra.

IV. THEORY

Since the standard theoretical formalism used in the analysis of nuclear Compton scattering experiments has been thoroughly discussed previously (e.g., Refs. [29,30]), only a brief summary will be given here. The elastic cross section for an incident photon energy E_γ and a scattering angle θ is defined by a total scattering amplitude $T(E_\gamma,\theta)$ such that $d\sigma/d\Omega=|T(E_\gamma,\theta)|^2$. At $\theta=0°$, this is connected to the total photoabsorption cross section (σ_γ) via a dispersion relation,

$$\mathrm{Re}[T(E_\gamma,0)]=\mathrm{Re}[T(0,0)]+\frac{2E_\gamma^2}{\pi}P\int_0^\infty\frac{\sigma_\gamma(E')}{E_\gamma^2-E'^2}dE', \tag{17}$$

TABLE II. Differential cross sections (lab frame) for the inelastic (4.44-MeV state) scattering of 84–105 MeV photons from ^{12}C. The first error is statistical and the second is systematic.

θ (deg)	$d\sigma^{inel}/d\Omega$ (nb/sr)
60	−0.6±5.1±6.1
90	8.6±3.2±4.6
120	20.0±3.8±4.4
150	16.4±4.0±4.2

and the optical theorem,

$$\mathrm{Im}[T(E_\gamma,0)]=\frac{E_\gamma}{4\pi}\sigma_\gamma(E_\gamma). \tag{18}$$

The total amplitude can be subdivided into four component amplitudes,

$$T(E_\gamma,\theta)=R_{GR}(E_\gamma,\theta)+R_{QD}(E_\gamma,\theta)+S^{(1)}(E_\gamma,\theta)+S^{(2)}(E_\gamma,\theta), \tag{19}$$

with two resonance amplitudes describing contributions from the collective nuclear excitations of the giant-multipole resonances $[R_{GR}(E_\gamma,\theta)]$ and quasideuteron excitations $[R_{QD}(E_\gamma,\theta)]$, and one- and two-body seagull amplitudes describing subnucleon and explicit meson degrees of freedom [$S^{(1)}(E_\gamma,\theta)$ and $S^{(2)}(E_\gamma,\theta)$]. In the $E_\gamma\to0$ limit, gauge invariance dictates that the total amplitude must satisfy the limit

$$T(0,\theta)=-\frac{Z^2}{A}\frac{e^2}{M}g_{E1}(\theta), \tag{20}$$

where Z and A are the proton and atomic numbers of the nucleus, M is the mass of the nucleon, and e is the proton charge ($e^2=1/137$). The electric-dipole angular distribution factor $g_{E1}(\theta)$ is given by

$$g_{E1}(\theta)=\vec{\epsilon}\cdot\vec{\epsilon}', \tag{21}$$

with $\vec{\epsilon}$ and $\vec{\epsilon}'$ being the polarization vectors of the incident and scattered photon. In the same $E_\gamma\to0$ limit, the one-body seagull term corresponds to Thomson scattering from point protons,

$$S^{(1)}(0,\theta)=-\frac{Ze^2}{M}g_{E1}(\theta), \tag{22}$$

and the limit, Eq. (20), constrains the form of the two-body seagull to be

$$S^{(2)}(0,\theta)=\frac{NZ}{A}\frac{e^2}{M}(-\kappa)\,g_{E1}(\theta). \tag{23}$$

The resonance amplitudes become [29]

$$R_{GR}(0,\theta)=\frac{NZ}{A}\frac{e^2}{M}(1+\kappa_{GR})g_{E1}(\theta), \tag{24}$$

$$R_{QD}(0,\theta)=\frac{NZ}{A}\frac{e^2}{M}\kappa_{QD}g_{E1}(\theta), \tag{25}$$

where N is the neutron number of the nucleus. κ_{GR} and κ_{QD} ($\kappa=\kappa_{GR}+\kappa_{QD}$) are the enhancement factors in the integrated sum of the dipole photoabsorption amplitude due to the giant-dipole resonance and quasideuteron excitations, respectively.

The dynamic parts of the resonance amplitudes are calculated by applying the dispersion relation [Eq. (17)] and the optical theorem [Eq. (18)] to the individual multipole and quasideuteron components of the photoabsorption cross section, and then multiplying by the appropriate angular factors. In addition to $g_{E1}(\theta)$, the magnetic dipole and electric quadrupole angular factors are also relevant,

$$g_{M1}(\theta)=(\vec{\epsilon}\times\hat{k})\cdot(\vec{\epsilon}'\times\hat{k}'), \tag{26}$$

$$g_{E2}(\theta)=\vec{\epsilon}\cdot\vec{\epsilon}'\hat{k}\cdot\hat{k}'+\vec{\epsilon}\cdot\hat{k}'\vec{\epsilon}'\cdot\hat{k}, \tag{27}$$

where $\hat{k}$ and $\hat{k}'$ are the direction vectors of the incident and scattered photons. In the case of the quasideuteron amplitude, the angular factor $g_{E1}(\theta)$ is also scaled by a two-body form factor, $F_2(q)$ (where $\vec{q}=\vec{k}-\vec{k}'$), introduced to account for the spatial distribution of nucleon pairs within the nucleus.

Modulating the LEX form of the nucleon amplitude by the nuclear-charge form factor, $F_1(q)$, the one-body seagull amplitude for a spinless nucleus below pion threshold is obtained,

$$\begin{aligned}S^{(1)}(E_\gamma,\theta)=&-\frac{Ze^2}{M}g_{E1}(\theta)F_1(q)\\&+AE_\gamma^2[\tilde{\alpha}_N g_{E1}(\theta)+\tilde{\beta}_N g_{M1}(\theta)]F_1(q)\\&+\vartheta(E_\gamma^4).\end{aligned} \tag{28}$$

The polarizabilities $\tilde{\alpha}_N$ and $\tilde{\beta}_N$ include possible medium modifications to the free-nucleon polarizabilities, $\overline{\alpha}_N$ and $\overline{\beta}_N$. Analogously, the energy-dependent part of the mesonic seagull amplitude can be parametrized in terms of exchange polarizabilities, $\delta\alpha$ and $\delta\beta$ [20],

$$\begin{aligned}S^{(2)}(E_\gamma,\theta)=&-\kappa\frac{NZe^2}{AM}g_{E1}(\theta)F_2(q)\\&+AE_\gamma^2[\delta\alpha g_{E1}(\theta)+\delta\beta g_{M1}(\theta)]F_2(q)\\&+\vartheta(E_\gamma^4).\end{aligned} \tag{29}$$

The dynamic parts of the one- and two-body seagull amplitudes are usually combined and expressed in terms of effective polarizabilities [22],

$$\begin{aligned}S(E_\gamma,\theta)&=S^{(1)}(E_\gamma,\theta)+S^{(2)}(E_\gamma,\theta)\\&=-\frac{e^2}{M}\left[ZF_1(q)+\kappa\frac{NZ}{A}F_2(q)\right]g_{E1}(\theta)+N(E_\gamma,\theta),\end{aligned} \tag{30}$$

where

$$N(E_\gamma,\theta)=AE_\gamma^2\left(1+\frac{E_\gamma^2}{\overline{E}^2}\right)F_1(q)[\tilde{\alpha}_{eff}g_{E1}(\theta)+\tilde{\beta}_{eff}g_{M1}(\theta)],$$

and $\overline{E}=270$ MeV is the $\vartheta(E_\gamma^4)$ correction prescribed in Ref. [29]. Since the seagull amplitudes are related to the non-nuclear excitations in the photoabsorption cross sections, the imaginary parts of the seagull amplitudes are zero below the pion threshold. The appropriate dispersion sum rule for the effective polarizabilities is

$$\tilde{\alpha}_{eff}+\tilde{\beta}_{eff}=\frac{1}{2\pi^2A}\int_{m_\pi}^{\infty}\frac{\sigma_\gamma^{tot}(E')-\sigma_\gamma^{QD}(E')}{E'^2}dE', \tag{31}$$

where the integral begins at m_π because again the seagull amplitudes are related to the non-nuclear excitations in the photoabsorption cross sections.

Taking the form for the total seagull amplitude to be that in Eq. (30), the only inputs in the theoretical calculation of the cross section are the form factors $F_1(q)$ and $F_2(q)$, the parametrization of the total photoabsorption cross section σ_γ^{tot}, and the effective polarizabilities $\tilde{\alpha}_{eff}$ and $\tilde{\beta}_{eff}$. The one-body charge form factor is calculated using the three-parameter Fermi (3PF) charge distribution of de Jager *et al.* [31],

$$\frac{n(r)}{n_0}=\frac{1+wr^2/c^2}{1+\exp[(r-c)/z]}, \tag{32}$$

where $w=-0.149$, $c=2.355$ fm, and $z=0.522$ fm. For the two-body form factor, whose form is much less certain, the commonly used phenomenological approximation, $F_2(q)=[F_1(q/2)]^2$, is employed.

The parametrization of the total absorption cross section is largely constrained by the data of Ref. [32]. Experimental uncertainties in this data, and in the location and strength of the electric quadrupole and quasideuteron components of the spectrum, admit some degree of latitude in choosing the parametrization that best fits the Compton scattering differential cross section. For a particular parametrization of the absorption data, scattering data at forward angles can be used to evaluate the sum $\tilde{\alpha}_{eff}+\tilde{\beta}_{eff}$. The sum can also be obtained from a calculation of the integral in Eq. (31), although this method of evaluation relies on averaging the scaled absorption data for different nuclei to cover the entire energy range of interest [17,29]. As was mentioned in the Introduction, a sum consistent with the corresponding free-nucleon sum $\overline{\alpha}_N+\overline{\beta}_N$ is generally assumed; use of such a sum for the effective polarizabilities is also consistent with both our scattering data at $\theta=35°$ and a reasonable parametrization of the absorption data. For convenience and ease of comparison

with the Lund ^{12}C results, the Lorentz lines listed in Table IV of Ref. [18] were used as a base parametrization of the absorption data. For completeness, an additional magnetic dipole ($M1$) Lorentz line (the parameters of which are given in Ref. [33]) was included to account for the 15.1-MeV excited bound state. Once an appropriate parametrization and a value for $\widetilde{\alpha}_{eff}+\widetilde{\beta}_{eff}$ have been determined, a fit to the angular distribution of the differential cross section with one parameter ($\widetilde{\alpha}_{eff}$) is performed.

Recently, a more complete theoretical study of the dynamic components of the mesonic seagull amplitude $S^{(2)}(E_\gamma,\theta)$ has been undertaken by Hütt and Milstein [23]. This study includes a calculation of the exchange polarizabilities $\delta\alpha$ and $\delta\beta$, and two dissimilar two-body form factors $F_2^{(1)}(q)$ and $F_2^{(2)}(q)$ scaling the static and dynamic parts of $S^{(2)}(E,\theta)$, respectively. Thus, by replacing $S(E_\gamma,\theta)$ in Eq. (30) with the more complete form of Eqs. (28) and (29), the effect on our results of using the theoretical inputs reported in Ref. [23] will also be explored.

V. RESULTS AND DISCUSSION

A. Elastic scattering

In analyzing our data, we first attempted to most closely compare our results to those of Lund [23]. This was done by using both, their value for the sum of the polarizabilities, $\widetilde{\alpha}_{eff}+\widetilde{\beta}_{eff}=14.0$, and their Lorentz-line parametrization of the absorption spectrum (with the additional $M1$ line mentioned above). Under these conditions, the polarizabilities that minimize the χ^2 in a fit to our 20 data points (five scattering angles for each of four energy bins) are

$$\widetilde{\alpha}_{eff}=7.0\pm0.2, \quad \widetilde{\beta}_{eff}=7.0\mp0.2. \tag{33}$$

The χ^2 of this fit with one free parameter is 28, with the corresponding reduced χ^2_ν being 1.5. The error in the polarizabilities given in Eq. (33) is that due to the statistical and systematic uncertainties (added in quadrature) in the cross sections, and corresponds to an increase of 1 in the χ^2. Fitting the Lund data at 75 MeV, we were able to reproduce their reported results of $\widetilde{\alpha}_{eff}=11.5$ and $\widetilde{\beta}_{eff}=2.5$, giving us confidence in the consistency of the analysis. Figure 4 compares theoretical curves calculated with both of the above sets of values for ($\widetilde{\alpha}_{eff},\widetilde{\beta}_{eff}$) to our data summed over the entire focal plane (94 MeV) and to the data of Häger *et al.* at 58 and 75 MeV. A direct comparison of our cross sections to those of Lund is not possible because of the different energies spanned by the two experiments. If, however, it is assumed that the theoretical model is reliable over the energy range of interest, Fig. 4 suggests that the discrepancy in the extracted polarizabilities is a consequence of our cross sections being larger at backward angles (relative to the forward angles) than those of Lund. A reduction of our cross sections at back angles of about 30%—roughly eight times the estimated uncertainty in these cross sections—would be necessary to obtain the Lund values. As had been stated in the Introduction, the polarizabilities extracted from the ^{16}O data

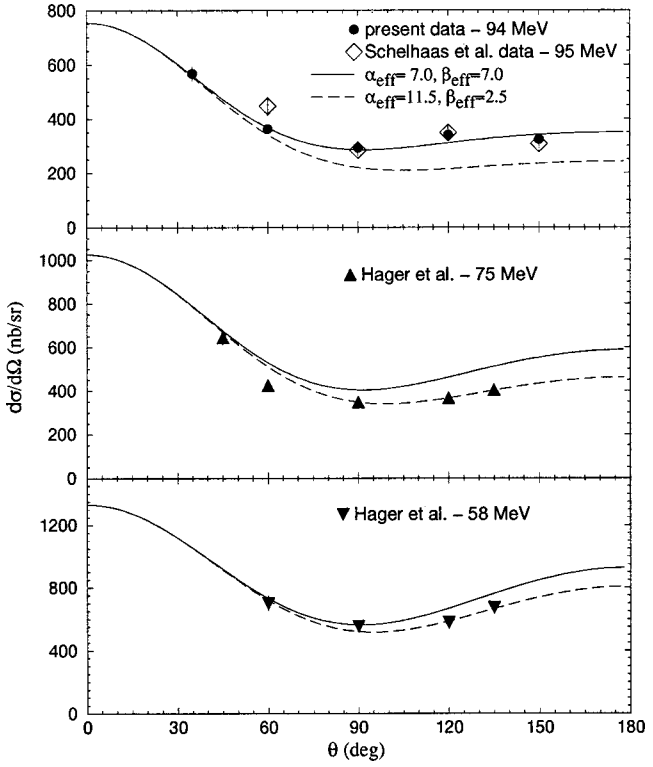

FIG. 4. Comparison of measured elastic-scattering differential cross sections to theoretical calculations. The error bars on the data represent the statistical and systematic errors added in quadrature.

of Feldman *et al.* [20] were also different than those suggested by the Lund ^{16}O data, and this difference also appears to result from a discrepancy in the backward angle cross sections. A reduction of approximately 30% in the cross section measured by Feldman *et al.* at $\theta=135°$ and $E_\gamma=74$ MeV would be required to reconcile that data with the Lund data at 75 MeV. We note that our data are consistent with the data of Schelhaas *et al.* [34] spanning a similar energy range as our experiment at scattering angles of $\theta=90°$, 120°, and 150°. The cross section of Schelhaas *et al.* at 60° is, however, significantly higher than ours. The Schelhaas *et al.* data are also depicted in Fig. 4, where five of their energy points have been averaged to give the points shown for the single energy of 95 MeV.

For the remaining analysis, we chose to use a sum of $\widetilde{\alpha}_{eff}+\widetilde{\beta}_{eff}=15.0$, which coincides with both the free-nucleon-averaged sum and the sum used by both Feldman *et al.* and Proff *et al.* To better fit our data at the forward scattering angle of $\theta=35°$, this choice for the sum suggested a small adjustment to the Häger *et al.* parametrization of the absorption spectrum: this could be accommodated by adjusting the height and width parameters of the existing $E1$ Lorentz lines and/or by changing the parameters of the quasideuteron line. The changes were not allowed to compromise the consistency of the parametrization with the absorption data of Ahrens *et al.* [32]. Examples of two such possible adjustments are depicted in Fig. 5, one with only the parameters of some of the $E1$ lines adjusted, and one with just the quasideuteron line scaled up by 15%. For comparison pur-

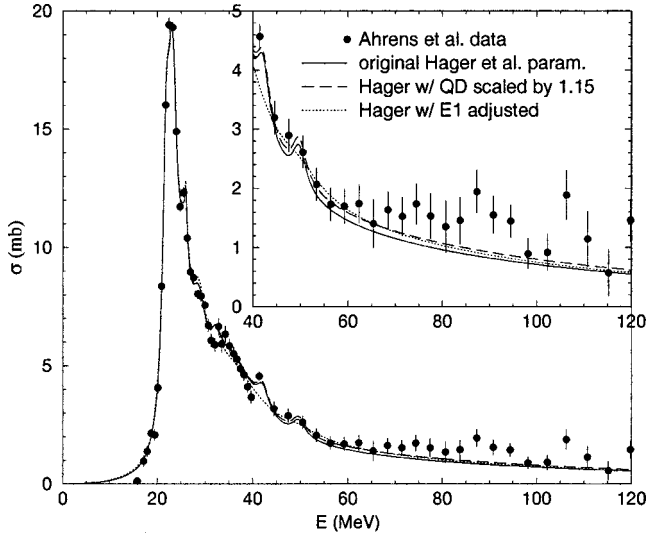

FIG. 5. Minor modifications to parametrizations of Häger *et al.* for the total absorption data of Ahrens *et al.*

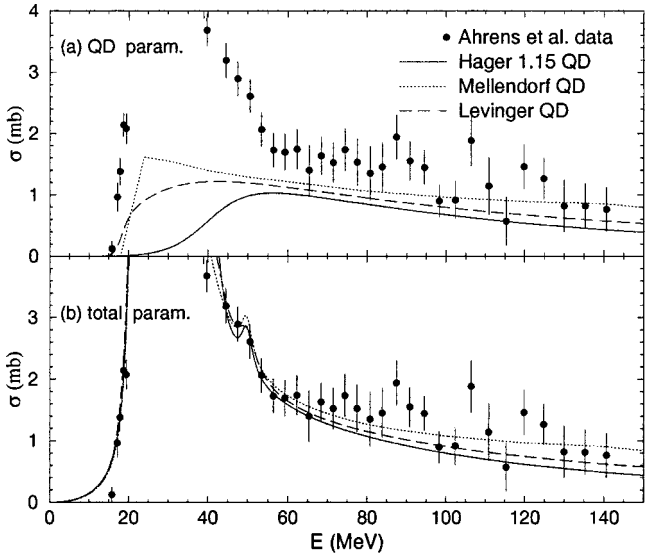

FIG. 6. Different models to parameterize total absorption data of Ahrens *et al*. The quasideuteron (QD) component (a) and the overall parametrization curve (b) are shown.

poses, the original parametrization of Häger *et al.* is also shown in Fig. 5. Using either of the two modified parametrizations shown, the fitted values for the polarizabilities become $\tilde{\alpha}_{eff}=8.2$, $\tilde{\beta}_{eff}=6.8$, with $\chi^2\simeq 30$ ($\chi^2_\nu=1.6$). More generally, we note that despite this latitude to adjust the parametrization in a reasonable fashion, the uncertainties in our data permit a range of only about ± 0.5 in $\tilde{\alpha}_{eff}$.

We now examine the model dependence of our extracted polarizabilities. In particular, the effects of the quasideuteron parametrization, the electric quadrupole strength, nuclear form factors, and meson-exchange parameters are discussed. In most cases, angular distributions from Häger *et al.* and our data were used to extract polarizabilities. The effects in question have inherent energy dependences and angular distributions from a fairly wide range of energies are required. The polarizabilities from the Häger *et el.* data and our data were treated as separate parameters of the fit because reconciliation of the two sets was never possible. However, this should not significantly affect the conclusions, since the change in polarizabilities with parametrization is the concern here. For the sake of orderliness, only polarizabilities and χ^2 from our data will be cited in the discussion. A summary of the results from this examination can be found in Table III, which also includes the effects on the polarizabilities from the data of Häger *et al.* not mentioned in the discussion. The effects can

TABLE III. Summary of the approximate effect of various model dependencies on the electric polarizability $\tilde{\alpha}_{eff}$ ($\tilde{\alpha}_{eff}+\tilde{\beta}_{eff}=15$) extracted from our data and that of Häger *et al.*

Model dependence	Present data	Häger *et al.*
Basic parametrization (e.g., $E1$)	± 0.5	± 0.9
QD parametrization	± 0.7	$+1.7$, -0.8
$E2$ parametrization	$+0.0$, -2.2	$+0.8$, -1.8
Nuclear charge form factor	$+1.7$	$+1.5$
Meson-exchange parametrization	-1.4	-0.8

be linearly cumulative resulting in large net variations. When all variations were taken into account, our data allowed a range of $\tilde{\alpha}_{eff}\approx 3-10.5$ and the data of Häger *et al.* allowed a range of $\tilde{\alpha}_{eff}\approx 8-16$.

1. Quasideuteron parametrization

Since the parametrization of the quasideuteron absorption is to some extent arbitrary, the dependence of our results on its shape and size are investigated. Generally, the energy dependence of the quasideuteron absorption above approximately 40 MeV is assumed to be similar to that of deuteron photodisintegration, while at lower energies Pauli blocking damps the cross sections. Three different parametrizations were used. In one case, the Häger *et al.* QD line was scaled up by 15%. Another used a piecewise linear function from the ^{16}O Compton scattering thesis of Mellendorf [35]. This was scaled by 0.75 for ^{12}C and the low-energy cutoff was shifted up to better match the low-energy absorption tail of ^{12}C. The third model was a modified Levinger [36] function of the form

$$\sigma_{QD}(E_\gamma)=L\frac{NZ}{A}\exp(-D/E_\gamma)\sigma_d(E_\gamma), \tag{34}$$

where $L=8$ is taken for the Levinger scaling factor, a damping parameter of $D=60$ MeV (as in Ref. [36]) is used, and σ_d is the deuteron photodisintegration cross section,

$$\sigma_d(E_\gamma)=62.4\frac{(E_\gamma-2.22\,\mathrm{MeV})^{3/2}}{E_\gamma^3}. \tag{35}$$

To better match the low-energy absorption tail, we also multiplied the form of Eq. (34) by a low-energy damping function, $\frac{1}{2}[1+\tanh(E_\gamma-18\ \mathrm{MeV}/2\ \mathrm{MeV})]$. Figure 6 shows the three quasideuteron parametrizations. The polarizabilities extracted from our data using these three parametrizations are

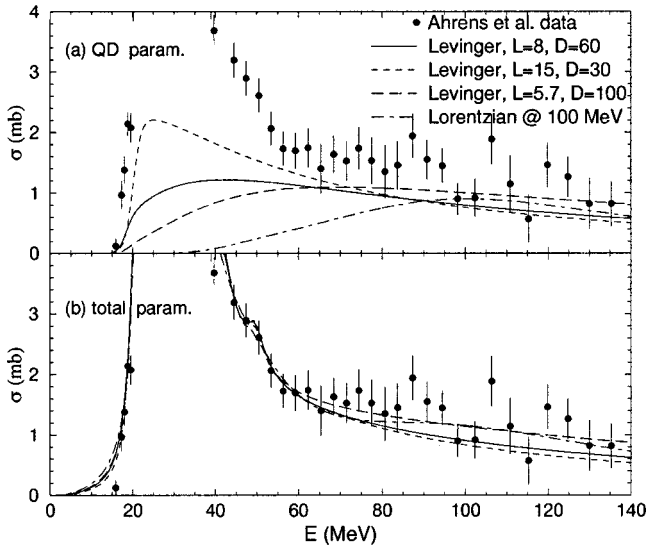

FIG. 7. Parametrization of total absorption data of Ahrens *et al.* with varied Levinger damping parameter *D*.

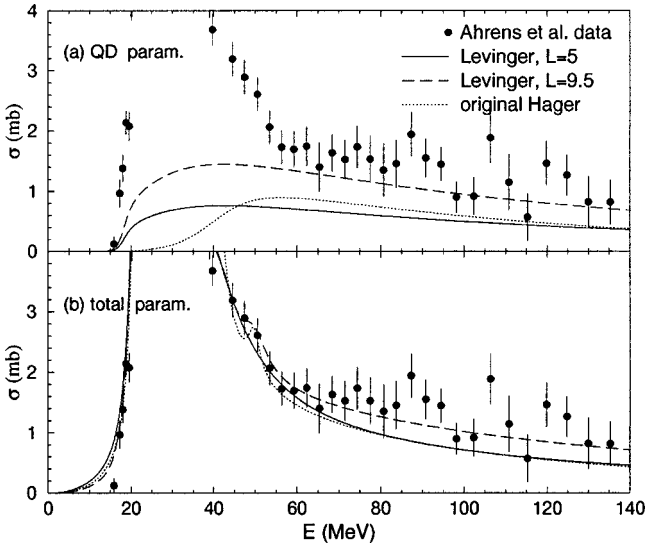

FIG. 8. Parametrization of total absorption data of Ahrens *et al.* with varied Levinger scaling parameter L for the strength of QD contributions. The original parametrization of Häger *et al.* is also shown for comparison.

nearly identical, yielding values of $\tilde{\alpha}_{eff}=8.0-8.2$. In each of these fits the parameters of the $E1$ Lorentz lines were adjusted to keep essentially unchanged both the parametrization of the absorption below 60 MeV and the fit to our data (averaged over the entire focal plane) at forward scattering angles.

The sensitivity of results to the shape of the QD absorption was further studied by considering different values of the parameter D in Eq. (34), which is not well defined. Figure 7 and Table IV compares Levinger parametrizations using $D=30$, 60, and 100 MeV. Compared to the resulting cross sections with $D=60$, they are flatter with respect to energy and peak at a higher energy with $D=100$, whereas, they decrease more quickly with energy and peak at a lower energy with $D=30$. Again, the extracted polarizabilities did not vary much, with the range of $\tilde{\alpha}_{eff}=7.8-8.1$. However, the fit to angular distributions using $D=100$ had a somewhat poorer χ^2 than with the $D=60$ and $D=30$ fits. The final QD parametrization shown in Fig. 7 is a Lorentz line peaked at 100 MeV (and damped at low energies), which is similar in shape to that used by Schelhaas *et al.* This gave an even worse fit to the data, yielding an unacceptable χ^2 of 71 ($\chi^2_\nu=3.7$). The inferiority of this last fit and (to a lesser extent) the fit using the $D=100$ parametrization suggests that QD strength is not peaked at high energies.

Since the uncertainties in the absorption data of Ahrens *et al.* allow a significant range of QD strengths, the dependence on the size of the QD was examined by varying the value of L in Eq. (34) ($D=60$ MeV). The QD component and corresponding total absorption cross section obtained from two parametrizations, one using $L=5$ and the other with $L=9.5$, are depicted in Fig. 8. As illustrated, the total absorption cross section with the $L=5$ parametrization is similar to the original Häger *et al.* parametrization in the QD region. Since they believed the ^{12}C absorption data to be unreasonably large in this region in comparison to the ^{16}O data, Häger *et al.* purposely selected their parametrization somewhat below the data. However, since it may also be possible that the ^{16}O data is low, or that the expected scaling of the QD cross sections by NZ/A does not strictly hold for these two nuclei, it also seems reasonable to consider a somewhat larger QD strength. The parametrization with $L=9.5$ represents $\approx 40\%$ more integrated strength between 70–140 MeV than the one with $L=5$. Despite this significant difference in strength, the extracted polarizabilities are similar, $\tilde{\alpha}_{eff}=7.8$ ($\chi^2=29, \chi^2_\nu=1.5$) and 8.3 ($\chi^2=37, \chi^2_\nu=1.9$) for the $L=5$ and $L=9.5$ cases, respectively. Although the uncertainties in the Ahrens *et al.* data permit even greater QD strength, further increases in L make it more difficult to get a good fit to both our data and to the Häger *et al.* data at 58 and 75 MeV; the $L=9.5$ fit to our data is already somewhat worse than the $L=5$ fit.

TABLE IV. Effect of varying the Levinger damping parameter D on polarizability extractions. Polarizability and χ^2 are from present data only.

D (MeV)	L	$\tilde{\alpha}_{eff}$	χ^2	χ^2_ν
30	5.7	7.8	29	1.5
60	8	8.0	32	1.7
100	15	8.1	44	2.3

Similar to the exercise described in Häger *et al.*, the final test of the QD model dependence on the extraction of the polarizabilities was performed by separating the $E1$ and QD absorption by attributing all absorption below/above some separation energy E_{QD} to $E1$/QD, and then varying the value of E_{QD}. A variation of $\approx \pm 0.7$ in $\tilde{\alpha}_{eff}$ was found by using a range of 30–70 MeV for E_{QD}.

The effect of the quasideuteron parametrization on the extracted polarizabilities seems to be small. Varying the shape and strength of the QD model resulted in the largest

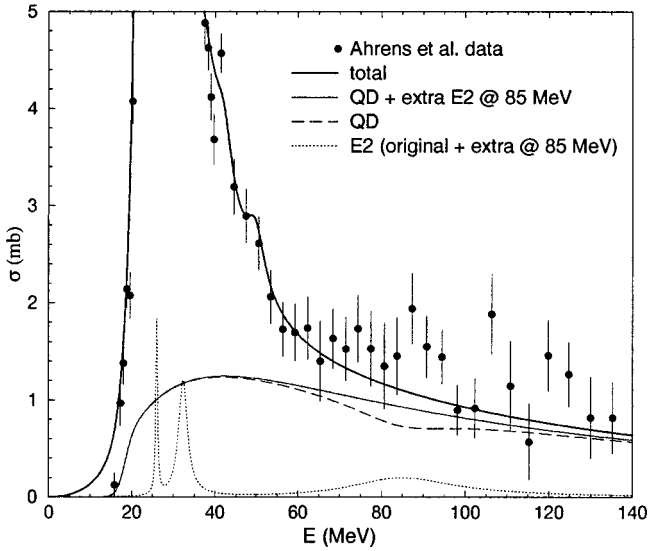

FIG. 9. Electric quadrupole ($E2$) and QD components of a parametrization of the total absorption data illustrating how extra $E2$ strength at 85 MeV was added.

variation of ± 0.7, which is comparable to the uncertainties of the measured polarizabilities of the free proton [Eq. (6)].

2. Electric quadrupole strength

In contrast to the fairly minor impact of the form of the QD parametrization on the extracted polarizabilities, the uncertainty in the quadrupole spectrum is more problematic. The asymmetry in the differential cross sections, with respect to $\theta = 90°$, is a manifestation of the $E1$-$M1$ interference ($\cos\theta$ dependence) and is used to distinguish between the electric and magnetic polarizabilities. However, it is also a feature of the $E1$-$E2$ interference ($\cos^3\theta$ dependence) and the location of the $E2$ strength is not well defined. The two Lorentz lines at 26.0 and 32.3 MeV [18], representing 0.72 total $E2$ TEWS (total energy weighted sums), used in the present analysis are based on $E2$ strength found by Schelhaas *et al.* [34], who also reported that this strength was consistent with that earlier found by Dodge *et al.* [37]. However, Wright *et al.* [38] suggested that most of the $E2$ strength is located above 50 MeV, while Taran and Gorbunov [39] also found significant quadrupole strength above 40 MeV.

We studied the effect of extra $E2$ strength by supplementing the original $E2$ Lorentz lines of Ref. [18] with one additional Lorentz line. Simply adding $E2$ strength resulted in poor fits and inconsistencies with total absorption cross sections. To improve the fits and remain consistent with the measured total absorption spectrum, this additional Lorentzian was accommodated by subtracting an equivalent Lorentzian from the $E1$ QD line (see Fig. 9), as done by Mellendorf [35]. Selecting various peak energies E_0 in the range of 40–115 MeV and various widths ($\Gamma = 5$, 15, or 30 MeV) for this extra $E2$ line, we then attempted to find a resonance height σ_0 that minimized the χ^2 in a fit to our scattering data. Distributions with various widths and peak energies below 95 MeV could be found that reduced the χ^2 below the $\chi^2 = 32$ ($\chi^2_\nu = 1.7, \tilde{\alpha}_{eff} = 7.8$) obtained without additional $E2$ strength. However, the Häger *et al.* data seemed to constrain any extra $E2$ resonance centered below 75 MeV to be broad (e.g., $\Gamma = 30$ MeV), as more concentrated strength tended to break the consistency between their 58- and 75-MeV points. An optimal fit to our data (see Fig. 10) was obtained using a broad, relatively small resonance centered around 85 MeV ($E_0 = 85$ MeV, $\sigma_0 = 0.2$ mb, $\Gamma = 30$ MeV, 0.14 TEWS). This gave $\tilde{\alpha}_{eff} = 6.3$ with $\chi^2 = 15$ ($\chi^2_\nu = 0.8$), a drop of 1.5 in $\tilde{\alpha}_{eff}$ and a factor of 2 drop in the χ^2 compared to the fit with no extra $E2$ strength. While not as optimal, increasing the $E2$ strength to $\sigma_0 = 0.3$ mb, at an energy of 85 MeV, would further reduce the value of $\tilde{\alpha}_{eff}$ to 5.6, while maintaining a good χ^2 of 18 ($\chi^2_\nu = 0.9$) and still maintaining a good fit to the data of Häger *et al.*

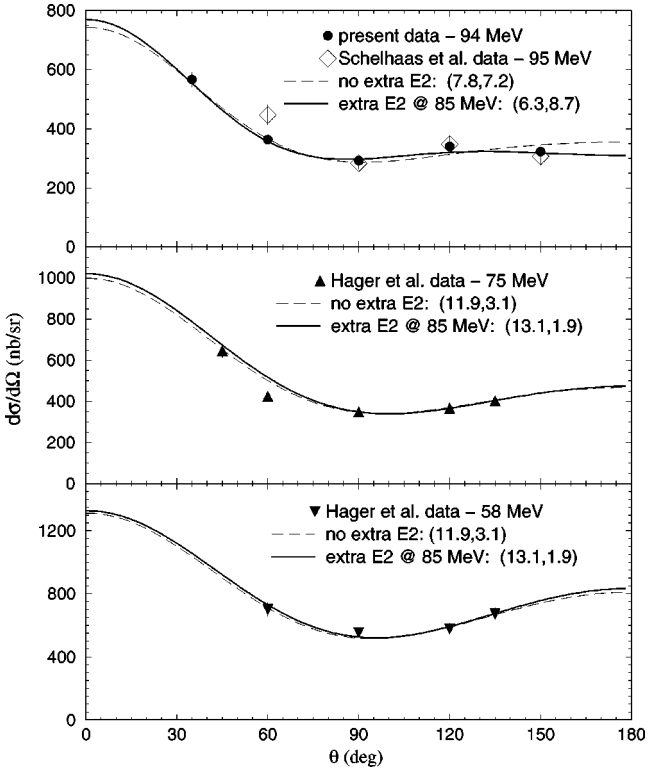

FIG. 10. Theoretical angular distributions with no extra $E2$ and when extra $E2$ strength is added at 85 MeV. The values of the polarizabilities used in the fits are given in the parentheses, ($\tilde{\alpha}_{eff}, \tilde{\beta}_{eff}$). The added $E2$ strength is consistent with both our data and that of Häger *et al.*

The effect of an $E2$ contribution above 95 MeV is illustrated in Fig. 11. Fits to our angular distributions at four energies with an extra $E2$ Lorentzian at 85 MeV ($E_0 = 85$ MeV, $\sigma_0 = 0.2$ mb, $\Gamma = 30$ MeV, 0.14 TEWS) were compared to fits with similar $E2$ strength at 105 MeV ($E_0 = 105$ MeV, $\sigma_0 = 0.2$ mb, $\Gamma = 30$ MeV, 0.09 TEWS) and fits with no extra $E2$ strength. Besides the differences in the $E2$ strength, a small variation was necessary in the scaling of the QD, which was allowed to make the fits at $\theta = 35°$ similar; the Levinger factor is $L = 8.2$, 7.7, and 7.8 for the ''$E2$ at 85 MeV,'' ''$E2$ at 105 MeV,'' and ''no extra $E2$'' parametri-

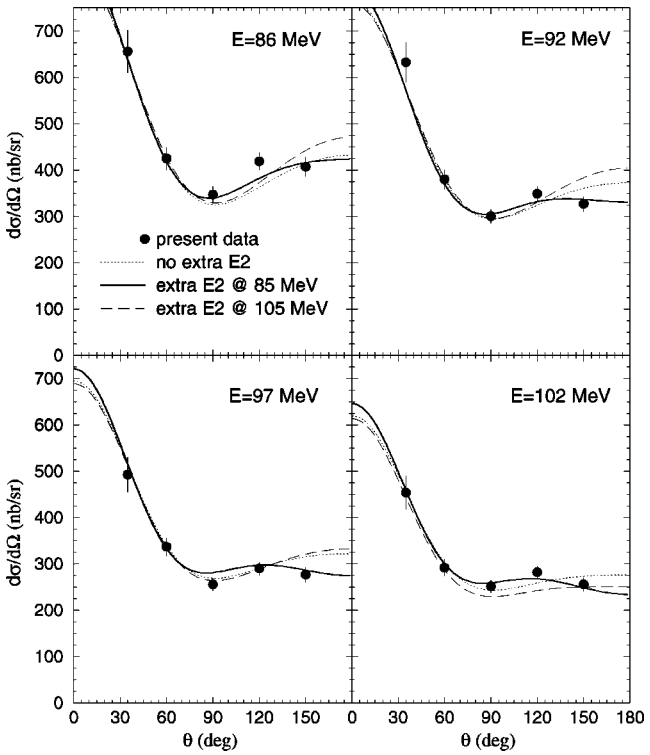

FIG. 11. Theoretical angular distributions showing effect of moving $E2$ from 85 MeV to 105 MeV. The calculation with no $E2$ is shown for comparison.

zations, respectively. Apart from that, the basic parametrizations were identical. The χ^2 of 46 ($\chi^2_\nu=2.4$) for the fit with the extra $E2$ at 105 MeV ($\tilde{\alpha}_{eff}=8.1$) indicates that the $E2$ strength centered at energies above the range spanned by our experiment are apparently inconsistent with the shape of our angular distributions (e.g., cross sections being higher at $\theta=120°$ than those at $\theta=150°$). While the existence of the extra $E2$ strength above 40 MeV is somewhat uncertain, the foregoing analysis does demonstrate that extracted polarizabilities from NCS on ^{12}C can vary widely if there are additional phenomena involved that are not included in the calculations.

Despite the degree of uncertainty in the parametrization of the total absorption cross section, and particularly its quasideuteron and electric-quadrupole components, we were unable to find a parametrization that gave a good fit to both our data and that of Häger *et al.* when using the same polarizabilities for both data sets. For parametrizations that gave acceptable fits to both sets individually, the extracted value of $\tilde{\alpha}_{eff}$ was approximately 2.5–7 lower in fits to our data than the corresponding Häger *et al.* value. We were thus unable to reconcile our cross sections with those of Häger *et al.* with the existing theoretical model.

The effect of additional electric-quadrupole strength on extracted polarizabilities can be significant. Our angular distribution strongly suggests the presence of this amplitude, as does the data of Schelhaas *et al.* The lower differential cross section at 150° was the key evidence of this in both data sets. Data limits the $E2$ peak energy between 55 and 95 MeV, favoring 85 MeV. There was no $E2$ parametrization that resulted in an increase in $\tilde{\alpha}_{eff}$, but a good fit with the $E2$ at 85 MeV changed it by -2.2. The energy and strength of this amplitude need to be determined. Finally, despite the degree of uncertainty in all of the parameters, it was not possible to reconcile our data and that of Häger *et al.* using the existing model.

3. Nuclear form factors and meson-exchange parameters

Our final consideration with respect to model dependence is the meson-exchange effect done by Hütt and Milstein. Using their form factors $F_1(q)$, $F_2^{(1)}(q)$, and $F_2^{(2)}(q)$ and exchange polarizabilities $\delta\alpha=-0.99$ and $\delta\beta=0.77$ for ^{12}C [23,30], the bound-nucleon polarizabilities resulting from a fit to our data (averaged over the entire focal plane) become $\tilde{\alpha}_N=9.6$, $\tilde{\beta}_N=5.4$.

However, when calculating their form factors, Hütt and Milstein used a somewhat different value for the parameter w of the three-parameter Fermi nucleon density function, Eq. (33), than has been used in the previous sections. Up to this point our calculations used a value of $w=-0.149$, whereas Hütt and Milstein used $w=-0.23$ in their calculations. Thus, to be consistent and to directly compare to the Hütt/Milstein model, a calculation using the more phenomenological model was performed using the 3PF with $w=-0.23$ to calculate $F_1(q)$ and $F_2(q)=[F_1(q/2)]^2$. This yielded an effective electric polarizability of $\tilde{\alpha}_{eff}=9.6$. The approximate relationship between $\tilde{\alpha}_{eff}$ and $\tilde{\alpha}_N$, with a given value for $\delta\alpha$, is

$$\tilde{\alpha}_{eff}\rightarrow\tilde{\alpha}_N+\delta\alpha\frac{F_2^{(2)}(q)}{F_1(q)} \tag{36}$$

[ignoring $\vartheta(E_\gamma^4)$]. Equation (36) allows a rough comparison between results with the two models, using $\delta\alpha=-0.99$, and the ratio $F_2^{(2)}(q)/F_1(q)$ averaging ≈ 1.4 for the three angles of 90°, 120°, and 150° at $E_\gamma=94$ MeV. The analogous effective polarizability from the Hütt/Milstein model is then $\tilde{\alpha}_{eff}\approx 8.2$, as compared to 9.6 from the the phenomenological model.

Another extraction with the phenomenological model, under the same conditions except using $w=-0.149$ resulted in $\tilde{\alpha}_{eff}=7.9$ compared to 9.6 using $w=-0.23$. So there is also a significant uncertainty due solely to the choice of parametrization for $n(r)$ (i.e., in the parametrization of the charge scattering form factor itself).

Figure 12 compares our scattering data to theoretical calculations done with the three different scenarios for the form factors: the Hütt and Milstein model with $w=-0.23$, the phenomenological model with $w=-0.23$, and the phenomenological model with $w=-0.149$. As illustrated, the shapes of the fits are similar in all three cases; thus, the angular distribution of the data cannot be used to distinguish between them. Since the three cases yield appreciably different values for the extracted polarizabilities, it is clear that the form factors must be better understood before such extraction can reliably be done.

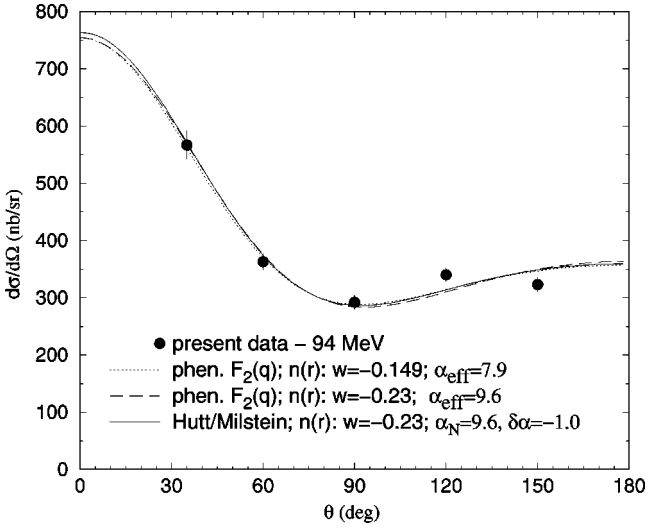

FIG. 12. Theoretical angular distributions calculated with different models for the form factors.

B. Inelastic scattering

The most recent inelastic scattering cross sections published in this energy range are the tagged photon measurements of Schelhaas *et al.* [34]. These are compared to the present results in Fig. 13 at 135°. Data at other angles have been transformed to this angle assuming the nearly isotropic angular distribution of Hayward [40],

$$\frac{d\sigma}{d\Omega} \propto 13 + \cos^2\theta. \tag{37}$$

The uncertainty in the data includes the uncertainties in line shape discussed earlier. Systematic errors are pessimistically added linearly to the statistical errors. These results significantly reduce the upper limit on the strength of the inelastic channel.

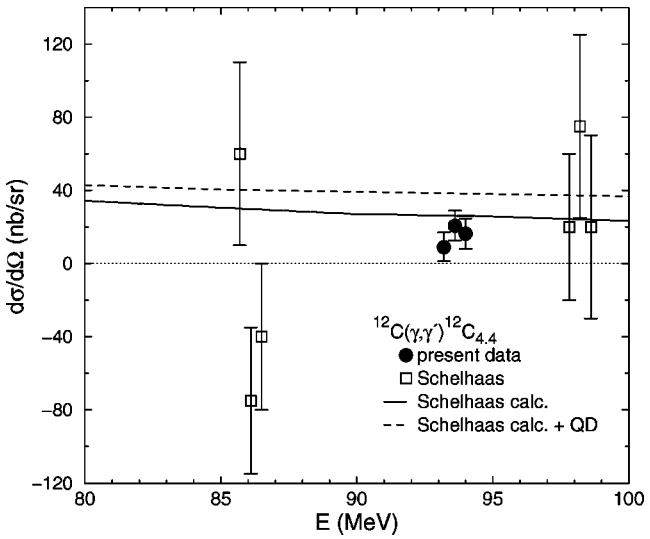

FIG. 13. Inelastic cross sections transformed to 135°. The present data points transformed from angles of $\theta = 90°$, 120°, and 150° are actually at the same incident photon energy, but have been displaced slightly for clarity.

Schelhaas *et al.* found that their data was reasonably described by their calculations, which followed the prescription of Hayward. They assumed that the ratio of the square of inelastic to elastic matrix elements, ρ_{inel}, was fairly energy independent. The magnitude of ρ_{inel} was constrained by the sum of elastic and inelastic cross sections matching previous inclusive cross sections. Schelhaas *et al.* also left open the question of whether quasideuteron intermediate states feed the inelastic channel. They assumed it did not (solid line in Fig. 13), but could not rule it out (dashed line in Fig. 13) due to relatively large uncertainties. The present results have significantly improved accuracy, and the largest value is slightly more than two standard deviations smaller than the QD inclusive calculation. This suggests that the QD intermediate states do not feed the inelastic channel if ρ_{inel} is energy independent. On the other hand, it is not clear if a 25% reduction in ρ_{inel} is impossible. Improved calculations and further measurements at other energies with similar precision as ours are necessary to establish the energy dependence and the importance of quasideuteron effects.

VI. CONCLUSION

Differential cross sections for nuclear Compton scattering from ^{12}C have been measured at scattering angles from 35° to 150° and energies from 84 to 105 MeV. Inelastic scattering and other background processes were clearly resolved in the energy spectra.

An attempt to analyze the data to extract bound-nucleon polarizabilities and possible medium modifications was severely hampered by ambiguities in models. Studies showed that due to model dependencies, our data permitted a range for the electric polarizability of $\tilde{\alpha}_{eff} \approx 3-10.5$, while the data of Häger *et al.* allowed a range of $\tilde{\alpha}_{eff} \approx 8-16$. With this degree of ambiguity, even the Häger *et al.* results could actually suggest some medium modification in contradiction to their own conclusions. While the effect of the poorly understood quasideuteron contribution was not significant, the question of additional $E2$ strength at higher energies has been shown to significantly affect the resulting polarizabilities. Furthermore, the shape of our angular distributions seems to strongly suggest the presence of that amplitude and places an upper limit on its energy of about 95 MeV, while Wright *et al.* imply a lower limit of 55 MeV. The apparent inconsistency of the relative levels of total absorption cross sections for carbon and oxygen between 60 and 130 MeV complicates the assessment of both the quasideuteron and $E2$ contributions and needs to be resolved. A confirmation of the presence of $E2$ strength between 55 and 95 MeV would significantly improve confidence in extracted polarizabilities. It is recommended that angular distribution measurements include far backward angles (e.g., 150°) in a wide range of energies (e.g., 40–110 MeV).

Yet another source of variability is the choice of the model and parametrization of the nuclear form factors, for which there is no sensitivity in angular distributions. In particular, the choice of w in the Fermi three-parameter model of charge distributions needs to be better constrained, and

then the explicit meson-exchange parametrizations such as the Hütt and Milstein model need to be reevaluated.

Finally, despite the variability of models and extracted polarizabilities, it was not possible to find a single value for the polarizabilities that fitted both the current data and the lower energy data by Häger *et al*. It is unlikely that this is due to the inability of the models to adequately describe the reaction at higher energies, since the current data includes cross sections at an energy only 11 MeV higher than the 75 MeV data of Häger *et al*. Furthermore, Schelhaas *et al.* were able to describe their data up to 140 MeV consistently with the existing models. It thus seems more probable that, as with Feldman *et al.*, there is an inherent discrepancy between the present cross section data and that of Häger *et al*. However, the model ambiguities make difficult any further assessment regarding medium modifications from any data set.

Inelastic scattering differential cross sections have been extracted for the 4.4-MeV excited state in ^{12}C. The data represent an improvement from previous measurements and suggest little quasideuteron intermediate-state contributions. These results demonstrate the feasibility of further measurements to establish the energy dependence of this channel and to compare to calculations of the quasideuteron contributions.

ACKNOWLEDGMENTS

One of the authors (B.J.W.) would like to thank A.I. Milstein and M.-Th. Hütt for supplying details of their calculations of the exchange parameters, and J. Ahrens for providing his data file for the photoabsorption from ^{12}C. We also express our appreciation to A. Nathan for illuminating discussions regarding the theoretical models and methods for interpreting the data. This work was supported in part by a grant from the Natural Science and Engineering Research Council of Canada.

[1] B.E. MacGibbon *et al.*, Phys. Rev. C **52**, 2097 (1995).
[2] J. Tonnison, A.M. Sandorfi, S. Hoblit, and A.M. Nathan, Phys. Rev. Lett. **80**, 4382 (1998).
[3] A.M. Baldin, Nucl. Phys. **18**, 310 (1960).
[4] D. Babusci, G. Giordano, and G. Matone, Phys. Rev. C **57**, 291 (1998).
[5] M.I. Levchuk and A.I. L'vov, Nucl. Phys. **A674**, 449 (2000).
[6] V.A. Petrun'kin, Fiz. Elem. Chastits At. Yadra **12**, 692 (1981) [Sov. J. Part Nucl. **12**, 278 (1981)].
[7] J. Schmiedmayer, P. Reihs, J.A. Harvey, and N.W. Hill, Phys. Rev. Lett. **66**, 1015 (1991).
[8] L. Koester *et al.*, Phys. Rev. C **51**, 3363 (1995).
[9] T.L. Enik, L.V. Mitsyna, V.G. Nikolenko, A.B. Popov, and G.S. Samosvat, Yad Fiz. **60**, 648 (1997) [Sov. J. Nucl. Phys. **60**, 567 (1997)].
[10] K.W. Rose *et al.*, Nucl. Phys. **A514**, 621 (1990).
[11] M. A. Lucas, Ph.D. thesis, University of Illinois, 1994.
[12] F. Wissman *et al.*, Nucl. Phys. **A660**, 232 (1999).
[13] N. Kolb *et al.*, Phys. Rev. Lett. **85**, 1388 (2000).
[14] D.L. Hornidge *et al.*, Phys. Rev. Lett. **84**, 2334 (2000).
[15] V. Bernard, N. Kaiser, and U.-G. Meisner, Int. J. Mod. Phys. E **4**, 193 (1995).
[16] G.G. Bunatyan, Yad. Fiz. **55**, 3196 (1992) [Sov. J. Nucl. Phys. **55**, 1781 (1992)].
[17] A. Baumann *et al.*, Phys. Rev. C **38**, 1940 (1988).
[18] D. Häger *et al.*, Nucl. Phys. **A595**, 287 (1995).
[19] M. Ludwig *et al.*, Phys. Lett. B **274**, 275 (1992).
[20] G. Feldman *et al.*, Phys. Rev. C **54**, R2124 (1996).
[21] K. Fuhrberg *et al.*, Nucl. Phys. **A591**, 1 (1995).
[22] S. Proff *et al.*, Nucl. Phys. **A646**, 67 (1999).
[23] M.-Th Hütt and A.I. Milstein, Phys. Rev. C **57**, 305 (1998).
[24] D.P. Wells, Ph.D. thesis, University of Illinois at Urbana-Champaign, 1990.
[25] B.J. Warkentin, M.Sc. thesis, University of Saskatchewan, 1999.
[26] J.M. Vogt *et al.*, Nucl. Instrum. Methods Phys. Res. A **324**, 198 (1993).
[27] J. Miller *et al.*, Nucl. Instrum. Methods Phys. Res. A **270**, 431 (1988).
[28] D.L. Hornidge, Ph.D. thesis, University of Saskatchewan, 1999.
[29] M. Schumacher, P. Rullhusen, and A. Baumann, Nuovo Cimento Soc. Ital. Fis. **100A**, 339 (1988).
[30] M.-Th Hütt, A.I. L'vov, A.I. Milstein, and M. Schumacher, Phys. Rep. **323**, 457 (2000); (private communication).
[31] C.W. deJager, H. de Vries, and C. de Vries, At. Data Nucl. Data Tables **14**, 479 (1974).
[32] J. Ahrens *et al.*, Nucl. Phys. **A251**, 479 (1975); (private communication).
[33] E. Hayward, in *Giant Multipole Resonances*, edited by S. Costa and C. Schaerf (Springer-Verlag, Berlin, 1977), p. 340.
[34] K.P. Schelhaas *et al.*, Nucl. Phys. **A506**, 307 (1990).
[35] K. E. Mellendorf, Ph.D. thesis, University of Illinois, 1993.
[36] J.S. Levinger, Phys. Lett. **82B**, 181 (1979).
[37] W.R. Dodge *et al.*, Phys. Rev. C **28**, 8 (1983).
[38] D.H. Wright *et al.*, Phys. Rev. C **32**, 1174 (1985).
[39] G.G. Taran and A.N. Gorbunov, Yad. Fiz. **6**, 1124 (1968) [Sov. J. Nucl. Phys. **6**, 816 (1968)].
[40] E. Hayward, Nat. Bur. Stand. (U.S.) Monograph No. 118 (U.S. GPO, Washington, D.C., 1970).